Available online at www.sciencedirect.com
SCIENCE DIRECT
Journal of Molecular Catalysis A: Chemical 243 (2006) 111–119
JOURNAL OF MOLECULAR CATALYSIS A: CHEMICAL
www.elsevier.com/locate/molcata

Characterization of Mn(III)porphyrin immobilized on modified silica surfaces by EXAFS spectroscopy: A promising tool for analysis of supported metalloporphyrin catalysts

Alba D.Q. Ferreira *, Fábio S. Vinhado, Y. Iamamoto *

Departamento de Química, FFCLRP, Universidade de São Paulo, Av. Bandeirantes 3900, CEP 14040-901, Ribeirão Preto, SP, Brazil

Received 25 August 2004; received in revised form 6 July 2005; accepted 16 July 2005
Available online 23 September 2005

Abstract

Herein we present the first Mn–K edge EXAFS spectra recorded for manganese(III)porphyrin catalysts containing [Mn{T(4-*N*-MePy)P}$(L)_n]^{5+}$ (where L = oxygenated or nitrogenated axial ligands, $n = 1$ or 2) grafted onto modified silica-surfaces with propylimidazole, IPG (**3**), sulfonatophenyl, $SiSO_3^-$ (**4**), and both, $SiSO_3^-$IPG (**5**), where T(4-*N*-MePy)P is the ligand 5,10,15,20-tetra(4-*N*-methylpyridyl)porphyrinate. From the data analysis and the refinement results, we have obtained the following structural information concerning to the coordination environment around the Mn(III) ion: four Mn–N at 2.00 Å and two Mn–N/O_{axial} at 2.26 Å for **3**; four Mn–N at 2.03 Å and two Mn–O_{axial} at 2.27 Å for **4**, and four Mn–N at 2.02 Å and two Mn–N/O_{axial} at 2.28 Å for **5**. Correlations of EXAFS data with UV–vis spectra pattern and other properties such as colors of the materials allowed distinguishing between materials **3**, **4** and **5**. Materials **4** and **5** belong to the same category, which involves ionic complex–support interaction. Furthermore, there are evidences for the coordination of the imidazolic ligand to the manganese(III) ion in **3** and **5** from qualitative analysis of XANES data. In the case of the catalyst **5**, bearing both sulfonate and imidazole as functional groups, we have suggested that the nature of the [Mn{T(4-*N*-MePy)P}$(L)_n]^{5+}$–support interaction is predominantly of ionic character, even though the existence of Mn–imidazole bonds can be detected.

Keywords: EXAFS; Manganese(III)porphyrin; Coordination environment; Bi-functional support; Functionalized silica

1. Introduction

Immobilization of metalloporphyrins to solid matrixes, such as silica [1] and chemically modified silica surfaces [2], zeolites [3] or organic polymers [4] have been carried out, preferentially, with the aim of obtaining more efficient catalytic systems for oxidations catalyzed by these metal complexes, which mimic the action of heme-enzymes (peroxidases [5] and cytochrome P450 [6]). This immobilization of metalloporphyrins to solid supports can influence the chemistry of these catalytic systems since the support provides an environment of reaction and can lead to site-isolation of the catalyst. Furthermore, the solid support provides a higher stability for the catalyst and possibility of recovery and reuse.

In spite of these advantages supplied by the solid support, and potential applications in the industrial field, there is a lack regarding the structural characterization of immobilized metalloporphyrins, namely, a higher understanding about the coordination environment of the metal ion, which would require information at molecular and atomic levels. Lindsay Smith and co-workers [7] studied, by UV–vis spectroscopy, resonance Raman and electron paramagnetic resonance (EPR), the coordination environment around central Fe in the materials constituted by the Fe-porphyrins $[Fe(TPFP)(L)_n]^+$ and $[Fe(TDCPP)(L)_n]^+$ [8] coordinatively bound to imidazole and pyridine groups on organic polymers (polystyrene imidazole and polyvinylpyridine) and on surface of silica (propylimidazole and butylpyridine). They

* Corresponding authors. Tel.: +55 16 602 3716; fax: +55 16 633 8151.
E-mail address: iamamoto@usp.br (Y. Iamamoto).

1381-1169/$ – see front matter © 2005 Elsevier B.V. All rights reserved.
doi:10.1016/j.molcata.2005.07.039

obtained evidence that Fe-porphyrins on the flexible organic polymers are all low-spin six-coordinate Fe(II) species and on the rigid chemically modified silica surfaces the Fe-porphyrins are five-coordinate and high spin.

All Mn(III)porphyrins are paramagnetic but they have an even number of unpaired electrons and hence their EPR is difficult to measure. Raman can distinguish various coordination environments for porphyrin complexes but cannot give accurate parameters. Moreover, spectral changes in the UV–vis spectrum caused by the coordination of ligands such as imidazole or pyridine are often subtle, thus most of the times they cannot be distinguished with reliance in the spectra of complexes immobilized in/on rigid solids, since the solid can raise some distortion or different interactions with the molecule of the metal-complex leading to some changes in the UV–vis spectrum [1b]. These properties make difficult a study of characterization at atomic-level for supported Mn(III)porphyrins, which have been reported as very efficient catalysts in several oxidation reactions by single oxygen donors, such as iodosylbenzene [1a,9], $KHSO_5$ [4a,10] or H_2O_2 [11]. In this sense, X-ray absorption spectroscopy (XAS) is a promising technique to characterize these Mn(III)complex-catalysts since it is a local structure probe, which can provide information about coordination number, bond length and oxidation state of the metal ion and does not require the presence of long-range order, allowing the analysis of non-crystalline samples, such as silica-based materials. However, in spite of the growing interest on the structure–activity correlation of catalysts containing immobilized Mn(III)porphyrin complexes, only few studies have used XAS technique to investigate Mn-porphyrin systems [12–15]. In the case of the materials prepared by the incorporation of MnTPP halides into a NAFION matrix, which consist of a perfluorinated polymer bearing sulfonate groups, Mn–K EXAFS (extended X-ray absorption fine structure) was useful to demonstrate the nature of the Mn(III)TPP–matrix interactions [13]. The stability of iron and copper complexes of the cationic porphyrin used in our studies has also been investigated by XAS techniques when immobilized on montmorillonite clay [16].

In this paper, we report EXAFS studies of the catalyst-materials [Mn{T(4-*N*-MePy)P}(L)]-IPG (**3**) [Mn{T(4-*N*-MePy)P}$(L)_2$]-$SiSO_3$ (**4**) and [Mn{T(4-*N*-MePy)P}(L)]-$SiSO_3$ (IPG) (**5**), which consist of the cationic complex [Mn{T(4-*N*-MePy)P}$(L)_2]^{5+}$ supported on modified silica IPG, $SiSO_3^-$ and $SiSO_3^-$ (IPG) (Fig. 1), in order to address the nature of the interaction between Mn(III)porphyrin and solid support and the coordination environment around the Mn(III) ion. In order to help the analysis of the supported catalysts, a previous characterization, by UV–vis, as well as EXAFS of the unsupported complexes [Mn{T(4-*N*-MePy)P}$(L)_n]Cl_5$ (**1**) and [Mn{T(4-*N*-MePy)P}(imidazole)$_2]Cl_4$ (**2**) have been carried out. According to our knowledge, this is the first work focusing on such approach to this class of materials. The complex [Mn{T(4-

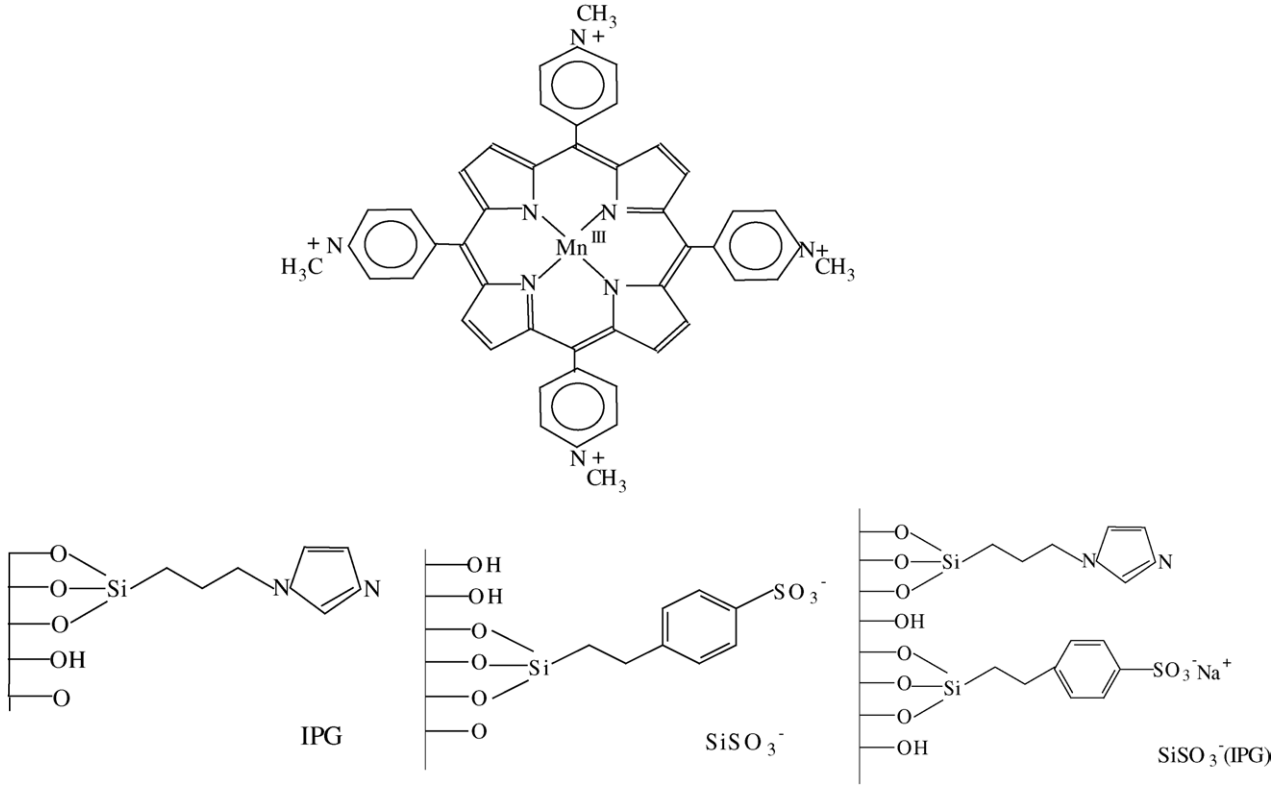

Fig. 1. [Mn{T(4-*N*-MePy)P}]$^{5+}$ and supports IPG, $SiSO_3^-$ and $SiSO_3^-$ (IPG).

N-MePy)P}$(H_2O)_2]^{5+}$ was chosen mainly since its crystallographic structure has been established [17].

2. Experimental

2.1. Reagents and materials

The precursor porphyrin T(4-*N*-MePy)PH_2 was purchased from Midcentury. All solvents and reagents were of commercial grade unless otherwise stated and were purchased from Merck, Aldrich and Mallinckrodt. Solvents were used as received.

2.1.1. Preparation of the complexes [Mn{T(4-N-MePy)P}$(L)_2$]Cl_5 and [Mn{T(4-N-MePy)P}(imidazole)$_2$]Cl_4

*2.1.1.1. [Mn{T(4-N-MePy)P}$(L)_2$]Cl_5 (**1**).* Manganese insertion into T(4-*N*-MePy)PH_2 was reached by heating the free-base porphyrin and $MnCl_2{\cdot}4H_2O$ at reflux in H_2O according methodology described by Adler et al. [18]. At the end of the reaction, Mn porphyrin obtained was separated by precipitation through the addition of NH_4PF_6 to the solution. Mn(III)porphyrin was converted to the chloride complex using a Dowex 1× 2–400, 2% cross-linking, 200–400 dry mesh ion exchange resin (Aldrich) with H_2O as eluent. The Mn(III)porphyrin obtained (λ_{max} = 464 nm in water in the UV–vis spectrum; 65% yield) gave one spot by TLC on alumina (methanol as eluent). Anal. Calcd. $C_{44}H_{36}N_8Cl_5Mn{\cdot}13H_2O$: C, 46.22; H, 5.48; N, 9.80. Found: C, 46.53; H, 5.70; N, 9.64.

*2.1.1.2. [Mn{T(4-N-MePy)P}(imidazole)$_2$]$(PF_6)_5$ (**2**).* Two-fold excess of imidazole was added to a solution of [Mn{T(4-*N*-MePy)P}$(L)_2$]$(PF_6)_4$ in MeCN that was kept under reflux for 7 h. The solvent was evaporated till dryness (λ_{max} = 468 nm in water in the UV–vis spectrum).

2.1.2. Solid supports

The solid supports IPG, $SiSO_3^-$ and $SiSO_3^-$ (IPG) (Fig. 1) were obtained and characterized previously [11b].

2.1.3. Preparation of supported manganese(III)porphyrins

Mn(III)porphyrins bound to the solid supports were obtained by stirring a solution of Mn(III)porphyrin in methanol with a suspension of support for about 30 min. The resulting catalysts [Mn{T(4-*N*-MePy)P}$(L)_n$]-supports were washed with methanol in a Soxhlet extractor overnight to remove unbound and weakly bound Mn(III)porphyrin. The solids were dried for 3 h at 100 °C. The loadings were quantified by measuring the amount of unloaded Mn(III)porphyrin, in the solvent washings, by UV–vis spectroscopy and indicated values 7.0–7.5 μmol/g of support for the three solid materials.

2.2. Instrumental

2.2.1. UV–vis spectra

UV–vis spectra were recorded on a Hewlett-Packard 8453 Diode Array UV–vis spectrophotometer. In the case of supported Mn(III)porphyrins, spectra were recorded in a 2 mm path length quartz cell, with the supported catalyst in a suspension of CCl_4. The "blank" was recorded previously and consisted of a support/CCl_4 suspension.

2.2.2. EXAFS data collection and analysis

The experiments were carried out on the XAS beam-line at the National Synchrotron Light Laboratory (LNLS). The operating current was between 200 and 100 mA (1.2 GeV). The line was equipped with a Si(2 2 0) double-crystal monochromators. The X-ray energy was calibrated using a Mn foil (6540 eV). The samples were obtained as fine power and packed into ∼1 mm sample holders between KAPTON foils. Data were collected in the fluorescence mode with a 15-element Ge solid state X-ray fluorescence detector [19]. The two unsupported complexes were analysed using thin samples to reduce the self-absorption effects. The absorption was related with the fluorescence signal divided by the incident beam ($A = F/I_0$). Three and two scans were obtained for the catalyst and reference samples, respectively. Each scan consisted of a set of multiple spectra and their averages were used for the analysis. The data reduction was carried out using the program WinXAS 1.2 [20] on a Pentium PC. To smooth these spectra the Golay–Savitzky algorithm was employed between 6440 and 7100 eV. A linear fit to points before the absorption edge was subtracted, and the data were normalized to absorption amplitude of unity at the edge by extrapolation of a second-order polynomial fit to data till 7085 eV. The data were transformed to a function of the wave vector k, where $k = [(E - E_0)2m_e/h^2]^{1/2}$. The Fourier transform of the k-space data gave peaks at R-space (pseudo-radial distance). The k-space data were truncated at ∼2.00 and ∼10.8 $Å^{-1}$ due a trace concentration of iron in the samples and because these spectra presented a low signal:noise ratio at higher k values. The FEFF 7.0 [21] input files (see Supporting Information S1) for the calculation of the backscattering amplitude $F(k)$, phase $\delta(k)$ and the photoelectron path λ were generated by TKATOMS [22] given a set of crystallographic coordinates of the complexes [MnT(4-*N*-MePy)P}$(H_2O)_2$]Cl_5 [17] and [Mn(TPP)(Py)Cl] [23].

$$\chi(k) = \sum_j \frac{N_j S_0^2 F_j(k)}{kR_j^2} e^{(-2k^2\sigma_j^2)} e^{\left(\frac{-2R_j}{\lambda}\right)} e^{\left(\frac{2}{3}\sigma_j'' k^4\right)} \times \sin\left[2kR_j + \delta_j(k) - \frac{4}{3}\sigma_j' k^3\right] \quad (1)$$

The simulation and refinement of the data were performed following the XAS Eq. (1). During the refinement of the first coordination shell single scatterings the Debye–Waller factors σ^2 were set between 0.001 and 0.008, the Mn–N_p dis-

tances R were constrained using the values of known XRD structures, whereas the coordination number N, the axial ligand distance and the S_0^2 factor were fixed. Usually, depending on the data quality, this technique allows estimating structural parameters with errors around 0.01–0.02 for interatomic distances and 5–20% for coordination numbers [24]. The complete fitting results and details on correlation and constrains are presented as Supporting Information (S2 to S6). The refinement profiles were expressed in terms of optimization curves (R factor versus χ_ν^2 (CHI reduced)) where R, the goodness-of-fit, is given as in Eq. (2) and χ_ν^2 is defined in Eq. (3):

$$R = \frac{\sum_{i=1}^{N} \left| y_{\text{exp}}(i) - y_{\text{theo}}(i) \right|}{\sum_{i=1}^{N} \left| y_{\text{exp}}(i) \right|} \times 100 \quad (2)$$

$$\chi_\nu^2 = \frac{1}{(N_i - np)\sigma^2} \sum_{i=1}^{N} [y_{\text{exp}}(i) - y_{\text{theo}}(i)] \quad (3)$$

3. Results and discussion

3.1. Characterizations of unsupported Mn(III)porphyrins [Mn{T(4-N-MePy)P}(L)$_2$]Cl$_5$ (1) and [Mn{T(4-N-MePy)P}(imidazole)$_2$]Cl$_4$ (2) by EXAFS spectroscopy

Complexes **1** and **2** were analysed by EXAFS before their immobilization on the solid supports. This characterization has been performed in order to help the analysis of the supported catalysts and the results are shown in Fig. 2 and Table 1. In order to determine the structural parameters, refinements were carried out for five- and six-coordinate structures, while the attenuation factor S_0^2 was kept as 0.85 or 1.0. The bond lengths were selected according to the optimization profiles, R factor and χ_ν^2 curves as a function of the distance between the manganese ion and **2** collected in the fluorescence mode. The interatomic distances are in Angstrom.

For the unsupported complex **1**, the Mn–$N_{average}$ distance obtained was 1.99 Å. The five-coordinate and six-coordinate fits using the structure of [Mn{T(4-*N*-MePy)P}$(H_2O)_2$]$^{5+}$ resulted in very close R values, however the minimum near 2.48 Å for the six-coordinate complex coincides with the minimum of χ_ν^2. The fitting results for the five-coordinate complex are given as Support Information (S2). The distance for this Mn–L_{axial} bond is close to the Mn–Cl distance in [Mn(TPP)(Cl)(py)] [23]. However, the use of its XRD structure to simulate and to refine the first coordination shell of this complex, did not afford good results (data not shown). Theoretically, it is possible to distinguish between O and Cl [25a], however as the resolutions of our experimental data are around $\Delta R \geq 0.2$ Å, these two shells will be not resolvable. Therefore, it can be suggested that both Cl^- and H_2O are present as axial ligands, with an elongated distance due to the effects of the electronic structure of six-coordinate Mn(III)porphyrins [26]. For the unsupported complex **2**, the same approach gave Mn–N distance at 1.99 Å and Mn–L_{axial} at 2.40 Å. The structure of [Mn(TPP)(Cl)(py)] was considered for the refinement, but the fit using the crystallographic data of [Mn{T(4-*N*-MePy)P}$(H_2O)_2$]$^{5+}$, having a six-coordinate structure, gave lower R factor and χ_ν^2 values by 6.4 and 14%, respectively. In the case of a five-coordinate environment, the R factor was reduced only by 3.5%, while the χ_ν^2 value increased by 11% (see Support Information S2 and S3).

3.2. Characterizations of supported Mn(III)porphyrins by UV–vis spectroscopy

As previously mentioned, the characterization of supported Mn(III)porphyrins by UV–vis spectroscopy provided, as a first approach, reliable information about the presence of the Mn(III)porphyrin on the supports due to the characteristic spectrum of these complexes [27]. The electronic spectra of the solid materials **3**, **4** and **5** are shown in Fig. 3.

A more detailed comparison of the three spectra in Fig. 3 indicates the B and C spectra are very similar, and spectrum A shows a slightly different pattern. From this consideration and based on the studies of Maclean et al. [28], who described studies of UV–vis for the material [Mn(TPP)]-Nafion and argued that a decrease in the value of R (a ratio between band V, here at 468 nm, and VI, here at 404 nm) is indicative of an increase in the six-coordination trend. The values of this ratio estimated for the supported catalysts are the following: [Mn{T(4-*N*-MePy)P}]-IPG ($r = 2.1$), [Mn{T(4-

Table 1
EXAFS fitting results for the first coordination sphere in the complexes **1** and **2**

	Mn–N	Mn–N/O_{axial}	N	E_0 (eV)	R factor	S_0^2	χ_ν^2	Δk (Å^{-1})	ΔR (Å)
Sample **1**[a]	1.99	2.48	6	6552.1	0.1331	0.85	274.87	2.1611–10.848	0.983–2.524
σ^2 (Å^2)	0.0054	0.008							
ΔE_0 (eV)	−1.91	−3							
Sample **2**[b]	1.99	2.40	6	6551.4	0.1167	0.85	504.76	2.063–11.0	0.7–2.50
σ^2 (Å^2)	0.0044	0.008							
ΔE_0 (eV)	0.6	3							

[a] XRD structural parameters used from the complex [Mn{T(4-*N*-Py)P}$(H_2O)_2$]Cl_5, from Ref. [17].
[b] XRD structural parameters used from the complex [Mn(TPP)(Py)Cl], from Ref. [23].

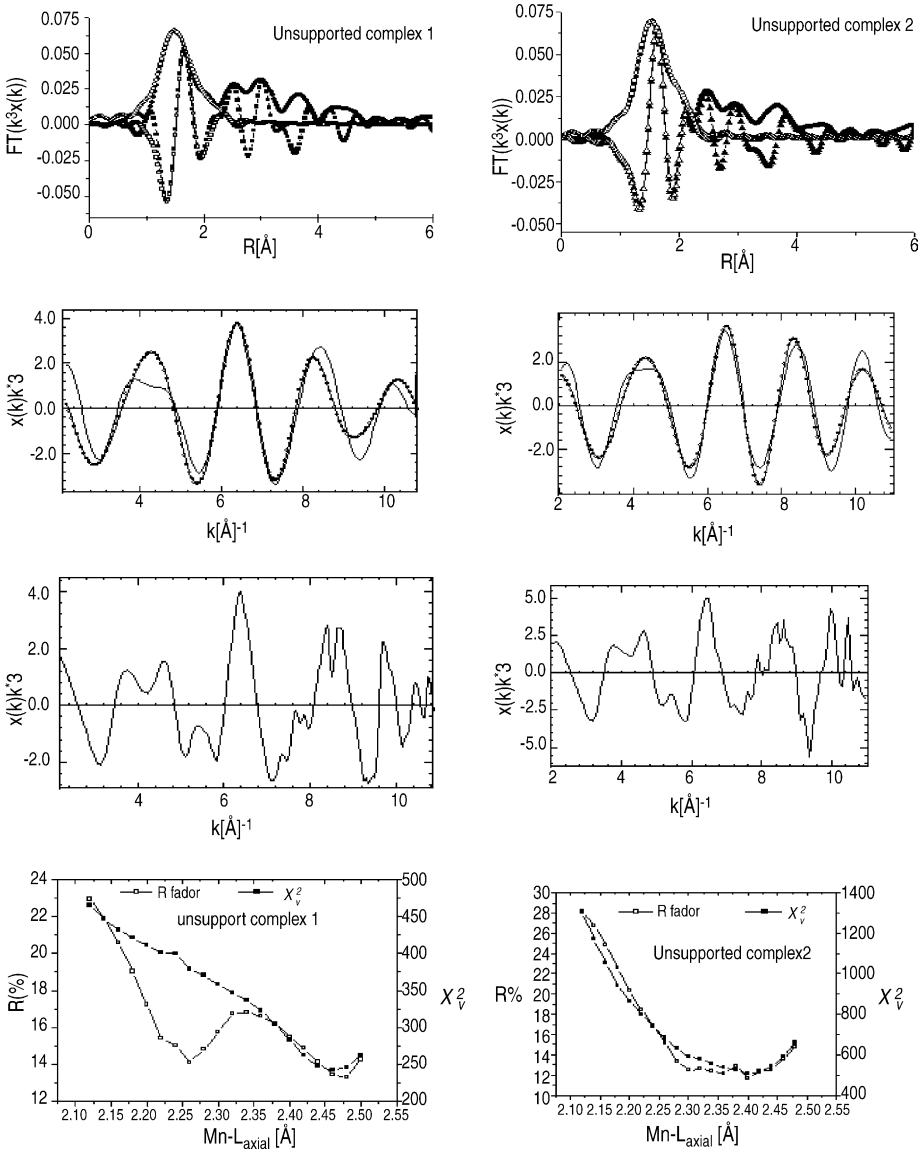

Fig. 2. Fourier transform k^3 (modulus + imaginary part) with the refined simulations for the first coordination shells (open circles, theoretical; solid lines, experimental) and the refinement profiles (black circles, χ^2_ν, open squares, R factor) with parameters given in Table 1: (a) Mn(III)porphyrin complex without imidazole (**1**) and (b) Mn(III)porphyrin complex + imidazole (**2**).

N-MePy)P}]-$SiSO_3$ ($r = 1.9$) and [Mn{T(4-*N*-MePy)P}]-$SiSO_3$ (IPG) ($r = 1.7$). Therefore, UV–vis study can suggest that materials **4** and **5** should have the Mn six-coordinate, while **3**, which does not contain anionic sulfonate groups on this surface, should have Mn ion, although six-coordinate, one imidazole as fifth ligand and probably the sixth weakly coordinated solvent ligand such as MeOH. The similarities between the UV–vis spectra of materials **4** and **5** can be understood if it is considered the involvement of same Mn–support ionic interactions and complexes geometry (Fig. 5). Other properties also confirm such similarities, for instance, **4** and **5** have the same color (reddish brown), whereas **3** is greenish brown. Also, as we will see through EXAFS data, the bond distances for both, **4** and **5** are too close.

3.3. Characterizations of supported Mn(III)porphyrins by EXAFS spectroscopy

The last step of the work, and the main target of it, was the analysis by EXAFS of the supported catalysts (Mn(III)porphyrins on modified silica surfaces) in order to understand the coordination environment around the central Mn(III) ion present in the solid materials.

Comparing the FTs, $\chi(k) \times k^3$ versus R (Å) shown in Figs. 2 and 4, a subtle similarity is observed between the spectra of [Mn{T(4-*N*-MePy)P}(L)]-IPG, [Mn{T(4-*N*-MePy)P}(L)]-$SiSO_3$ (IPG) and unsupported complex **2** in the region of the second coordination sphere single-scattering and multiple-scattering, while the spectra of [Mn{T(4-*N*-

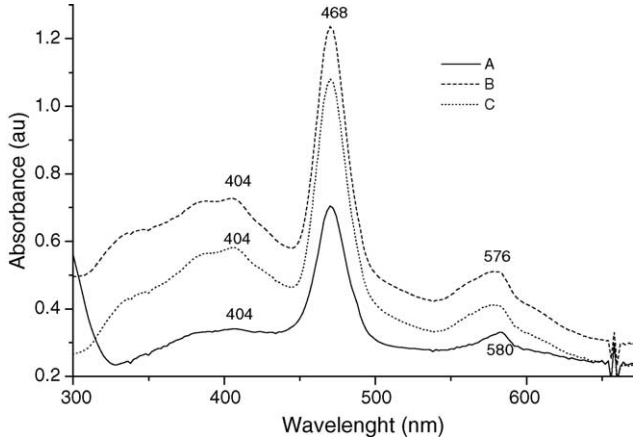

Fig. 3. UV–vis spectra of: (A) [Mn{T(4-*N*-MePy)P}]-IPG, **3**, (B) [Mn{T(4-*N*-MePy)P}]-$SiSO_3$ (IPG), **5** and (C) [Mn{T(4-*N*-MePy)P}]-$SiSO_3$, **4** as a suspension of CCl_4.

MePy)P}$(L)_2$]-$SiSO_3$ and unsupported complex **1** are closely related.

These results suggested that in the materials **3** and **5** the Mn(III)porphyrin is bound to the matrix through the nitrogen of the imidazole ring of the silica-support. On the other hand, the EXAFS analysis suggests that in **4** the Mn(III)complex is bound to the silica-support by ionic interactions, with the two axial positions occupied by oxygen atoms. In order to confirm this hypothesis, the refinement of the first shell was carried out applying the same approach used for the unsupported complexes. The FT peaks related to the contributions of the first coordination shells were simulated using the atomic coordinates of the two six-coordinate complexes mentioned before. Keeping the axial ligand distance, the coordination number and the attenuation factor S_0^2 fixed, each refinement was carried out for a given Mn–L_{axial} distance by varying the Debye–Waller factor, the Mn–N distances and E_0 parameters during the fit. The refinement results are displayed in the form of optimization profiles (*R* factor versus χ_ν^2 as depicted in Fig. 5). The refinement results for the first coordination spheres are shown in Table 2. It is worth pointing out that the differences in χ_ν^2 values are related mainly to the concentration of the sample, since in the unsupported complexes the concentration of manganese is higher than in the catalyst materials, what results in higher values of χ_ν^2 for the unsupported samples.

From the XRD structure of [Mn(TPP)(Py)Cl] the distances Mn–$N_{average}$, Mn–N_{axial} and Mn–Cl are 2.01, 2.44 and 2.467 Å, respectively [23]. In the structure of the [Mn{T(4-*N*-MePy)P}$(H_2O)_2$]Cl_5 the Mn–Naverage distance is 2.01 Å and the Mn–O is 2.22 Å [17]. Initially, the refinement of the parameters for the materials **3** and **5** were performed using the XRD coordinates of the [Mn(TPP)(Py)Cl] without Cl^- as the sixth ligand. In the case of **3**, the six-coordinate model gave the deepest minimum at 2.26 Å with *R* factor of 17% that is 18% lower than for the five-coordinate complex (Support Information S4). However, the best fit results for **5** were obtained with the XRD parameters of [Mn{T(4-

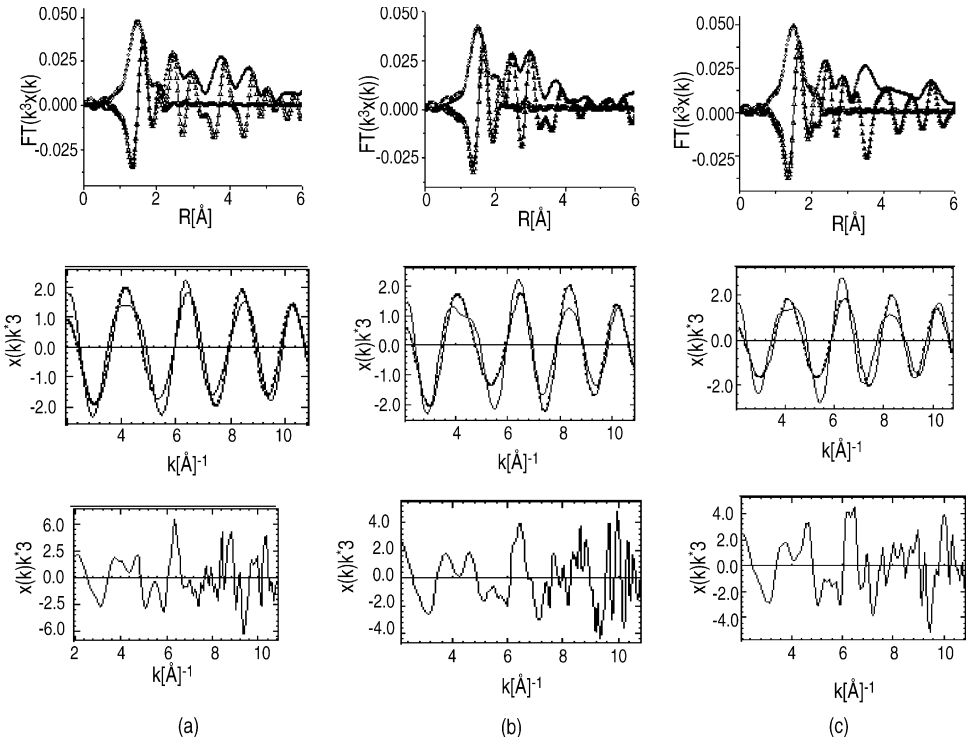

Fig. 4. Fourier-transformed k^3 (modulus + imaginary part) with the refined simulations for the first coordination shells (top panel), back-transforms of the refined shells (middle panel) and EXAFS × k^3 signals with parameters given in Table 2. (a) IPG (**3**), (b) $SiSO_3^-$ (**4**) and (c) $SiSO_3^-$ (IPG) (**5**) (open circles, theoretical; solid lines, experimental).

N-MePy)P}$(H_2O)_2$]Cl_5, decreasing the *R* factor and χ^2_ν by 33 and 22%, respectively. Comparing the fits with coordination numbers 5 and 6, it was observed that the six-coordinate structure reduced the *R* factor by 27% (see Support Information S6). The similarity between the Mn–$N_{average}$ distances, 2.03 Å for **4** and 2.02 Å for **5**, that are longer than the average distances found in six-coordinate Mn(III)porphyrins, is an indication that the $SiSO_3^-$ bearing supports leads to a distortion of the porphyrin ring. The difference of ±0.02 Å between the Mn–L_{axial} distances for **3**–**5** is in the range of typical systematic error in EXAFS analysis [24]. Even though is not possible to distinguish the origin of the oxygen atom by this EXAFS analysis, this Mn–O distance is found in the structure of [Mn(TPP)$(H_2O)_2$]ClO_4 [29]. The solvent used for the immobilization of the complex on to the matrix surface was MeOH, then its presence as axial ligand cannot be ruled out, since in the reported XRD structure of [Mn(TPP)$N_3(CH_3OH)$] the Mn–O distance is 2.329 Å [30]. As pointed by Maclean et al. [13], the competition between the oxygen atoms from the support and from the solvent for the axial positions should not be excluded, although in our examples the anionic ligands will interact, most likely, with the cationic functional groups of the porphyrin ring.

In the case of **4**, the material covered only with sulfonate groups, the best fitting result (*R* = 18.30%) was achieved considering that the Mn(III) coordination environment is formed by six atoms, while setting a five-coordinate model increased this agreement factor by 36% (see Support Information S5). The addition of Cl^- as axial ligand did not improve the refinement (data not shown). If these results are compared with those from the previous section, the main differences in the structural parameters, Mn–$N_{average}$ at 1.99 Å with longer

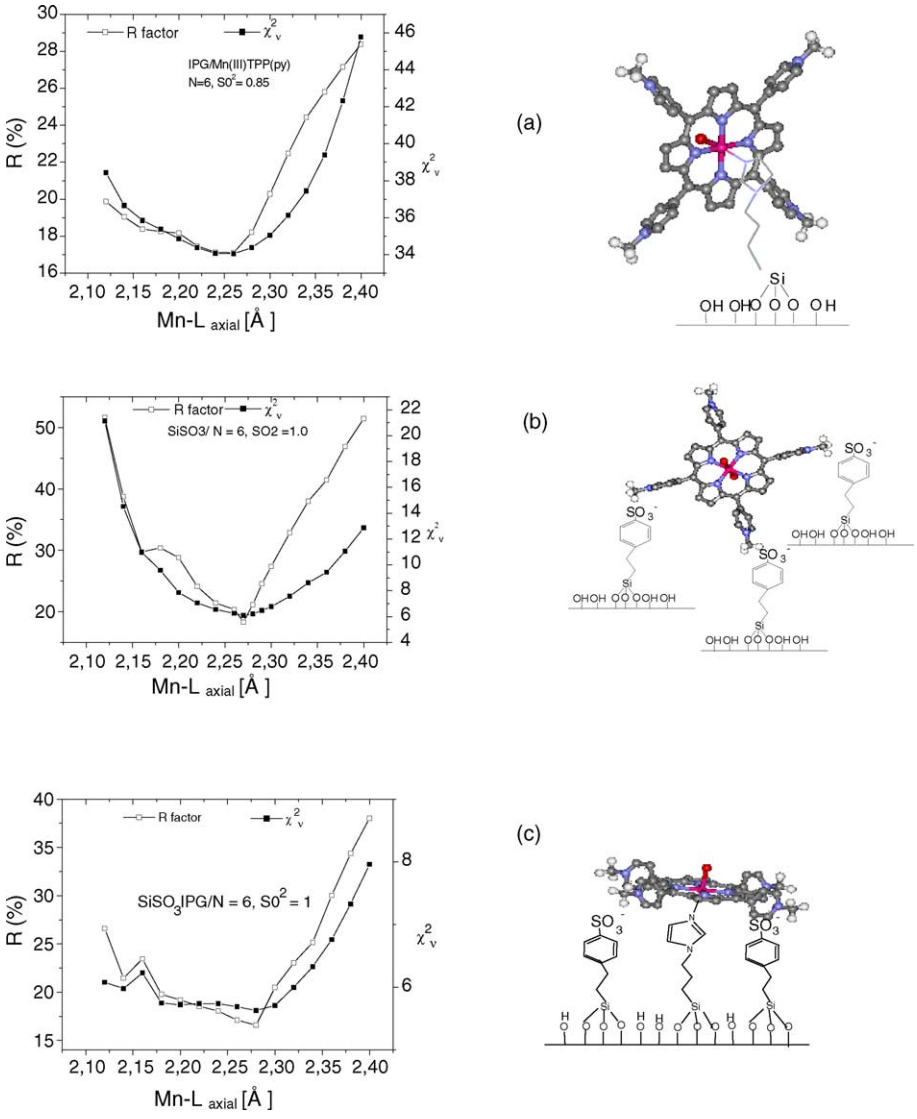

Fig. 5. Optimization profiles of the refined simulations for the first coordination shells whose parameters are given in Table 2: (a) IPG, (**3**), (b) $SiSO_3^-$ (**4**), and, (c) $SiSO_3^-$ (IPG) (**5**).

Table 2
EXAFS fitting results for the first coordination sphere in the supported catalysts **3**–**5** collected in the fluorescence mode

	Mn–N	Mn–N/O_{axial}	*N*	E_0 (eV)	*R* factor	S_0^2	χ_ν^2	Δk (Å^{-1})	ΔR (Å)
Sample **3**[a]	2.00	2.26	6	6551.5	0.1710	0.85	34.052	2.0892–10.852	0.7172–2.444
σ^2 (Å^2)	0.0055	0.0023							
ΔE_0 (eV)	1.03	1.96							
Sample **4**[b]	2.03	2.27	6	6552.6	0.1830	1.0	6.0854	2.154–10.865	0.7172–2.474
σ^2 (Å^2)	0.008	0.008							
ΔE_0 (eV)	1.7117	−3							
Sample **5**[b]	2.02	2.28	6	6552.6	0.1670	1.0	5.57	2.1335–10.80	0.728–2.40
σ^2 (Å^2)	0.0066	0.008							
ΔE_0 (eV)	0.1234	−3							

The interatomic distances are in Angstrom.
[a] XRD structural parameters used from the complex [Mn(TPP)(Py)Cl], from Ref. [23].
[b] XRD structural parameters used from the complex [Mn{T(4-*N*-Py)P}$(H_2O)_2$]Cl_5, from Ref. [17].

M–L_{axial} distances, suggest that the immobilization of the cationic Mn(III)porphyrin complex leads to a distortion of its structure.

The qualitative analysis of the XANES data (Support Information S7) points to the presence of the coordinated imidazole ring for the materials **3** and **5**, since it is known that this region of the XAS spectra is more sensitive to the multiple scattering than the short-range EXAFS structures [25]. The multiple scattering effects from the Mn–imidazole bond should be the reason for the characteristics signals [31] observed in the higher energy part of the spectra of **3** and **5**.

According to the previous considerations, some other properties, such as the UV–vis studies, colors of these materials and their resistance against leaching when washed with methanol in a Soxhlet system, also point for the kind of Mn(III)porphyrin–support interaction in these materials. For instance, **4** and **5** have the same color (reddish brown), whereas **3** is greenish brown. In addition, **4** and **5** undergo 1 and 2% of leaching when washed with methanol in Soxhlet extractor for ∼8 h, while **3** presents 5% of leaching under the same conditions [11b]. Therefore, these characteristics put the materials **4** and **5** at a same category since they suggest that in both the Mn(III)porphyrin–support interaction occurs rather by ionic binding through positive charges present on the *N*-methylpyridyl groups of the Mn(III)complex and the negative charges of the sulfonatophenyl groups present on the solid support and in both the coordination number should be the same. On the other hand, in the solid [Mn{T(4-*N*-MePy)P}$(L)_n$]-IPG **3** the immobilization Mn(III)porphyrin-support is mainly due to the interaction via coordinative binding of the imidazole groups present on the support and Mn(III) complex.

4. Conclusions

The correlation of the XAS data with UV–vis spectra pattern and some properties such as color and the resistance of these materials during Soxhlet extractions, allowed us to address the kind of interaction between the cationic [Mn{T(4-*N*-MePy)P}$(L)_n$]$^{5+}$ and the solid supports IPG (**3**), $SiSO_3^-$ (**4**) and $SiSO_3^-$ (IPG) (**5**). In [Mn{T(4-*N*-MePy)P}(L)]-IPG (**3**), the Mn(III)porphyrin is bound to the support by coordinative bonding between imidazole groups and the Mn(III), characterized by greenish-brown color and its corresponding UV–vis spectrum. Conversely, [Mn{T(4-*N*-MePy)P}$(L)_2$]-$SiSO_3$ (**4**) and [Mn{T(4-*N*-MePy)P}(L)]-$SiSO_3$ (IPG) (**5**) are reddish-brown and, in addition, present very similar UV–vis spectra. The Mn(III)porphyrin–support interaction occurs by ionic interactions, through the positive charges of the 4-*N*-methylpyridyl moieties and the sulfonatophenyl residues of the support. In the case of [Mn{T(4-*N*-MePy)P}(L)]–$SiSO_3$ (IPG) (**5**) the predominant Mn(III)porphyrin–support interaction is ionic, but, in addition, there are also molecules of [Mn{T(4-*N*-MePy)P}(L)]$^{5+}$ that are coordinated to the imidazole from the support. Furthermore, it is possible to infer that the Mn–$N_{average}$ distances from 1.99 Å for unsupported Mn(III)porphyrins **1** and **2**, 2.00 Å for the catalyst **3** going to 2.03 Å for **4** and 2.02 Å for **5**, can be interpreted as the presence of distortions in the porphyrin ring systems in these last ones, due to the ionic nature of the interaction with the supports.

We expect to extent this EXAFS study to other Mn(III)porphyrin catalysts prepared in our lab, whose catalytic profiles showed a remarkable influence of the imidazole coordination on the selectivity of oxidation reactions of hydrocarbons by simple oxygen atom donors.

Acknowledgements

We thank Anna Paula Sotero and Aline Y. Ramos from XAS beam line at LNLS (National Laboratory of Synchrotron Light, Brazil) for the technical support and suggestions during the data collection. Financial support from CNPq, CAPES, LNLS (partially) and FAPESP are gratefully acknowledged.

Appendix A. Supplementary data

Supplementary data associated with this article can be found, in the online version, at 10.1016/j.molcata.2005.07.039.

References

[1] (a) O. Leal, D.L. Anderson, R.C. Bowman, F. Basolo, R.L. Burwell, J. Am. Chem. Soc. 97 (1975) 5125;
(b) P.R. Cooke, J.R. Lindsay Smith, J. Chem. Soc. Perkin Trans. 1 (1994) 1913;
(c) L. Barloy, J.P. Lallier, P. Battioni, D. Mansuy, Y. Piffard, M. Tournoux, J.B. Valim, W. Jones, New J. Chem. 16 (1992) 71;
(d) K.J. Ciuffi, H.C. Sacco, J.C. Biazzotto, O.A. Serra, O.R. Nascimento, E.A. Vidoto, C.A.P. Leite, Y. Iamamoto, J. Non-Cryst. Solids 273 (2000) 100.

[2] (a) F.S. Vinhado, P.R. Martins, A.P. Masson, D.G. Abreu, E.A. Vidoto, O.R. Nascimento, Y. Iamamoto, J. Mol. Catal. A: Chem. 188 (2002) 141;
(b) M.D. Assis, J.R. Lindsay Smith, J. Chem. Soc. Perkin Trans. 2 (1998) 2221.

[3] (a) F. Bedioui, Coord. Chem. Rev. 144 (1995) 39;
(b) I.L.V. Rosa, C.M.C.P. Manso, O.A. Serra, Y. Iamamoto, J. Mol. Catal. A: Chem. 160 (2000) 199.

[4] (a) D. Pattou, G. Labat, S. Defrance, J.L. Séris, B. Meunier, New J. Chem. 13 (1989) 801;
(b) H.C. Sacco, Y. Iamamoto, J.R. Lindsay Smith, J. Chem. Soc. Perkin Trans. 2 (2001) 181;
(c) J.W. Huang, W.J. Mei, J. Liu, L.N. Ji, J. Mol. Catal. A: Chem. 170 (2001) 261;
(d) E. Brulé, Y.R. de Miguel, Tetrahedron Lett. 43 (2002) 8555.

[5] (a) T.L. Poulos, in: K.M. Kadish, K.M. Smith, R. Guilard (Eds.), The Porphyrin Handbook, vol. 4, Academic Press, San Diego, 2000, p. 189;
(b) P.J. O'Brien, Chem.–Biol. Interact. 129 (2000) 113;
(c) P. Jones, J. Biol. Chem. 276 (2001) 13791.

[6] (a) P.R. Ortiz de Montellano (Ed.), Cytochrome P450: Structure, Mechanism and Biochemistry, Plenum, New York, 1995;
(b) D.G. Kellner, S.C. Hung, K.E. Weiss, S.G. Sligar, J. Biol. Chem. 277 (2002) 9641;
(c) S. Yoshioka, T. Tosha, S. Takahashi, K. Ishimori, H. Hori, I. Morishima, J. Am. Chem. Soc. 124 (2002) 14571.

[7] P.R. Cooke, C. Gilmartin, G.W. Gray, J.R. Lindsay Smith, J. Chem. Soc. Perkin Trans. 2 (1995) 1573.

[8] [Fe(TPFP)]$^{+}$: 5,10,15,20-tetrakis(pentafluorophenyl)porphyrinato iron(III) [Fe(TDCPP)]+: 5,10,15,20-tetrakis(2,6-dichlorophenyl)porphyrinato iron(III).

[9] (a) C. Gilmartin, J.R. Lindsay Smith, J. Chem. Soc. Perkin Trans. 2 (1995) 1573;
(b) Y. Iamamoto, M.D. Assis, K.J. Ciuffi, C.M.C. Prado, B.Z. Prellwitz, M. Moraes, O.R. Nascimento, H.C. Sacco, J. Mol. Catal. A: Chem. 116 (1997) 365.

[10] S. Campestrini, B. Meunier, Inorg. Chem. 31 (1992) 1999.

[11] (a) M.A. Martinez-Lorente, P. Battioni, W. Kleemis, J.F. Bartoli, D. Mansuy, J. Mol. Catal. A: Chem. 113 (1996) 343;
(b) F.S. Vinhado, C.M.C. Prado-Manso, H.C. Sacco, Y. Iamamoto, J. Mol. Catal. A: Chem. 174 (2001) 279.

[12] V. Gotte, J. Goulon, C. Goulon-Ginet, A. Rogalev, C.R. Natoli, K. Perie, J.M. Barbe, R. Guilard, J. Phys. Chem. B 104 (2000) 1927.

[13] A.L. Maclean, G.J. Foran, B.J. Kennedy, Inorg. Chim. Acta 268 (1998) 231.

[14] K. Ayougou, E. Bill, J.M. Charnock, C.D. Garner, D. Mandon, A.X. Trautwein, R. Weiss, H. Winkler, Angew. Chem. Int. Ed. Eng. 34 (1995) 343.

[15] O. Bortolini, M. Ricci, B. Meunier, P. Friant, I. Ascone, J. Coalon, Nouv. J. Chem. 10 (1986) 39.

[16] K.A. Carrado, S.R. Wasserman, Chem. Mater. 8 (1996) 219.

[17] S. Prince, F. Korber, P.R. Cooke, J.R. Lindsay Smith, M.A. Mazid, Acta Crystallogr. Sect. C 49 (1993) 1158.

[18] A.D. Adler, F.R. Longo, J. Org. Chem. 32 (1967) 476.

[19] R.A. Barrea, A.P. Sotero, E. Tamura, A.Y. Ramos, H.C.N. Tolentino, Book of Abstracts of the 12th Meeting of Users of the LNLS Campinas, 2002, p. 136.

[20] T. Ressler, J. Synchrotr. Radiat. 5 (1998) 118.

[21] J.J. Rehr, R.C. Alberts, Phys. Rev. B 41 (1990) 8139.

[22] B. Ravel, J. Synchrotr. Radiat. 8 (2001) 314.

[23] J.F. Kirner, W.R. Scheidt, Inorg. Chem. 14 (1975) 2081.

[24] S.J. Gurman, J. Synchrotr. Radiat. 2 (1995) 56.

[25] (a) J.E. Penner-Hahn, Coord. Chem. Rev. 190–192 (1999) 1101;
(b) J. Goulon, C. Goulon-Ginet, V. Gotte, in: K.M. Kadish, K.M. Smith, R. Guilard (Eds.), The Porphyrin Handbook, vol. 7, Academic Press, San Diego, 2000, p. 79.

[26] W.R. Scheidt, in: K.M. Kadish, K.M. Smith, R. Guilard (Eds.), The Porphyrin Handbook, vol. 3, Academic Press, San Diego, 2005, p. 5.

[27] M. Gouterman, in: D. Dolphin (Ed.), The Porphyrins, Academic, New York, S. Francisco, London, 1978, p. 62.

[28] A.L. Maclean, R.S. Armstrong, B.J. Kennedy, J. Raman Spectrosc. 26 (1995) 981.

[29] M.M. Williamson, C.L. Hill, Inorg. Chem. 26 (1987) 4155.

[30] V.W. Day, B.R. Stults, E.L. Tasset, R.O. Day, R.S. Marianelli, J. Am. Chem. Soc. 96 (1974) 2650.

[31] A.H. de Vries, L. Hozoi, R. Broer, Int. J. Quant. Chem. 91 (2003) 57.